JOURNAL OF GUIDANCE, CONTROL, AND DYNAMICS
Vol. 33, No. 4, July–August 2010

Optimization of Circularly Towed Cable System in Crosswind

Paul Williams*
Delft University of Technology, 2629 HS Delft, The Netherlands

DOI: 10.2514/1.45241

The dynamics of aerial tethers towed in circular paths by an orbiting aircraft have been studied extensively. Typically, the atmosphere is assumed to be stationary with respect to the ground so that stable steady-state solutions are possible for certain combinations of system parameters. This paper presents a numerical approach for minimizing the disturbance of a crosswind on the periodic solution of the cable tip using a combination of towpoint manipulation and tether reeling. A discrete lumped parameter cable representation is used to simulate the physics of the cable system. Periodic solutions are generated for a range of towpoint motions including elliptical orbits. The required angular velocity of the aircraft to maintain constant airspeed is derived. Numerical results show that steady-state wind effects can be compensated for by flying the aircraft in an elliptical orbit upwind of the target point in combination with reeling the cable or flying on an inclined orbit.

Nomenclature

a	=	semimajor axis of elliptical orbit, m
$\boldsymbol{a}$	=	inertial acceleration of cable in rotational coordinate system, m/s^2
C	=	origin of rotational coordinate system
C_D	=	cable drag coefficient
C_DA	=	projected drag area of cable tip, m^2
C_L	=	cable lift coefficient
d	=	cable diameter, m
e	=	orbit eccentricity
$\boldsymbol{e}_L$	=	unit vector in lift direction
$\boldsymbol{e}_D$	=	unit vector in drag direction
$\boldsymbol{F}$	=	sum of external forces on cable in rotational coordinate system, N
g	=	gravity at sea level, 9.81 m/s^2
h_d	=	oscillation amplitude of aircraft in vertical plane, m
H	=	mean aircraft altitude, m
l_j	=	length of jth cable element, m
L_d	=	amplitude of length oscillation, m
m_j	=	mass of the jth cable element, kg
O	=	origin of inertial coordinate system
p	=	semilatus rectum of ellipse, $a(1 - e^2)$
r	=	orbit radius of aircraft, m
$\boldsymbol{r}$	=	position vector of cable in rotational coordinate system, m
T	=	tension in cable, N
$\boldsymbol{v}$	=	inertial velocity of cable in rotational coordinate system, m/s
$\boldsymbol{v}_j^{\text{rel}}$	=	velocity of jth cable element relative to air
T_p	=	orbital period, sec
V_T	=	true airspeed of aircraft, m/s
V_w	=	wind speed parallel to inertial x-axis, m/s
x_c	=	position of aircraft orbit origin along inertial $\boldsymbol{x}$-axis, focus of elliptical orbit, m
x_{tip}	=	position of cable tip on inertial $\boldsymbol{x}$-axis, m
y_c	=	position of aircraft orbit origin along inertial $\boldsymbol{y}$-axis, focus of elliptical orbit, m
y_{tip}	=	position of cable tip on inertial $\boldsymbol{y}$-axis, m
z_{tip}	=	position of cable tip on inertial $\boldsymbol{z}$-axis, m
α_j	=	generalized coordinate of jth cable element, rad
β_j	=	generalized coordinate of jth cable element, rad
κ	=	$1 + e\cos\theta$
θ	=	angle of aircraft relative to periapsis of ellipse, rad
θ_0	=	angle of periapsis of ellipse relative to inertial x axis
θ_d	=	phase of aircraft vertical oscillation relative to peripasis, rad
θ_L	=	phase of cable reeling relative to periapsis, rad

Received 2 May 2009; revision received 1 March 2010; accepted for publication 1 March 2010.

*Department of Aerospace Engineering. 1/4 Maylands Avenue, Balwyn North, VIC 3104, Australia. Member AIAA.

I. Introduction

THE dynamics of aerially towed cable systems have been of interest for several decades [1–9]. Potential uses of such technology ranges from towing aerial decoys and terrain-sensing, through to pickup and delivery of payloads [10]. Although the dynamics of aerial tethers have been studied extensively, there are comparatively fewer studies dealing with control of such systems. In particular, control is typically viewed from the point of view of the attitude, or altitude control of the towed body [11–14]. Such control is typically implemented via aerodynamic control surfaces on the towed-body. This approach becomes ineffective, however, for systems towed in a circular path because the relative velocity of the towed-body with respect to the wind is almost nonexistent under ideal circumstances. Hence, other control strategies are necessary.

This paper is concerned with the dynamics and control of a towed cable system flying closed orbital patterns. In the limiting case of an aircraft flying a circular orbit relative to a stationary atmosphere, the cable takes on a steady-state configuration when viewed from a rotational frame attached to the aircraft. Practical development of such a system could potentially allow extraction of supplies or injured personnel for wartime or peacetime support, or delivery of supplies to remote areas [15]. In previous studies on this topic, the atmosphere has been assumed to remain stationary relative to the aircraft. However, in the presence of a crosswind, the cable tip tends to oscillate in the vertical plane and move away from the relative equilibrium position obtained for no crosswind disturbances. It is therefore of considerable practical interest to assess the means by which such crosswinds can be compensated for. This is the goal of this work.

Previous studies of the dynamics of cables towed in circular paths have almost exclusively focused on relative equilibria and their corresponding stability [16]. Indeed, much of the earlier work has looked extensively at multivalued solutions and the system dynamics for high rotational velocities [5–9]. For a system towed from an aircraft, however, many of the stability problems such as cable flutter (neglecting effects such as vortex shedding) are unlikely to occur due to the relatively low angular velocities involved. In [16], a literature review of many of the earlier studies is provided. Furthermore, a possible method for enhancing the stationary motion by attaching a

high-drag device along the cable was investigated. Reference [17] studied the transient dynamics of the cable due to aircraft flight-path manipulation and optimized the transition from straight flight to circular flight so as to achieve rapid convergence of the cable tip to the desired equilibrium position. The effects of a crosswind were examined for a particular case by Murray [18], who used an inversion procedure to obtain the required aircraft motion to compensate for the winds. However, this process is unstable because of the very large aerodynamic gradient on the cable, and the method does not give a smooth motion for the aircraft. The effects of a crosswind were examined in [19], which studied periodic solutions for the towed system. The effects of noncircular (i.e., elliptical) orbits, and inclined circular orbits was also studied. Very little literature exists on the control of the system in the presence of crosswinds. In fact, [20,21] deal with the problem of damping wind induced oscillations of the cable by changing the aircraft bank angle as a function of heading using fuzzy logic. In this feedback control approach, wind oscillations are measured through oscillations in the cable tension. However, control of the system focused on maintaining high verticality, rather than accurate positioning of the cable tip.

This paper presents a study of the direct optimal control of an aerial-towed cable system. Specifically, focus is on systems nominally towed in circular orbits. Control of the cable tip is sought in the presence of steady crosswinds so as to keep the tip as close to the ideal center as possible. When crosswinds are present, steady-state configurations are not possible. Instead, periodic solutions occur with the cable tip varying in horizontal and vertical position. If the aircraft maintains its original circular orbit relative to the ground, then the aerodynamic force gradient can cause a significant perturbation to the position of the cable tip. The goal of this paper is to numerically study the form of optimal solutions for keeping the cable tip as close to the desired position as possible. This is achieved by a combination of changing the tether length and manipulating the aircraft orbit. Furthermore, periodicity constraints are also enforced so that the aircraft could potentially repeat the same control strategy over many orbits.

II. Mathematical Model

In this work, the cable system is modeled by a series of masses connected via frictionless rigid links. This model is similar to the ones presented in [16,17], except that the longitudinal extension of the cable is neglected. Although the longitudinal extension of the cable could have an effect on the resulting dynamics, it is neglected here to remove any high frequency vibrations from the problem formulation. This allows simulations to be conducted with larger time steps than would be allowed if the higher frequency oscillations were present. It also makes numerical computations of optimal solutions less sensitive to the initial guess.

A. Coordinate Frames

The cable dynamics are described in a rotating coordinate system that rotates with the aircraft's translational motion $(\boldsymbol{x}_1, \boldsymbol{x}_2, \boldsymbol{x}_3)$, centered at C. The origin of the coordinate system is described relative to an inertial coordinate system centered at O, $(\boldsymbol{x}, \boldsymbol{y}, \boldsymbol{z})$. The origin of the rotating system is given by the coordinates (x_c, y_c, H) as shown in Fig. 1.

The cable is discretized into n point mass elements. Each lumped mass is described by the relative spherical coordinates (l_j, α_j, β_j), where l_j is the length of the jth segment, and α_j and β_j are the two angles defined in Fig. 1, i.e., β_j is a rotation about the $\boldsymbol{x}_1$ axis, and α_j is a rotation about the intermediate $\boldsymbol{x}_2$ axis. The cable elements are numbered from 1 for the link closest to the aircraft, through to n, where the position of m_n represents the position of the towed body or cable tip.

In [22], the precursor to this paper, the equations of motion were derived using Kane's equations. This has some advantages in that one does not need to determine the cable tension as part of the dynamic solution. However, for solving the optimal control problem defined later in this paper, the computational burden becomes the dominant consideration. When Kane's equations are used, one must solve a system of linear equations at each time step, with a $2n \times 2n$ matrix. The approach adopted in this work, based on Newton's second law, requires only the solution of a $n \times n$ matrix at each time step, with the added advantage that the equations are less cumbersome.

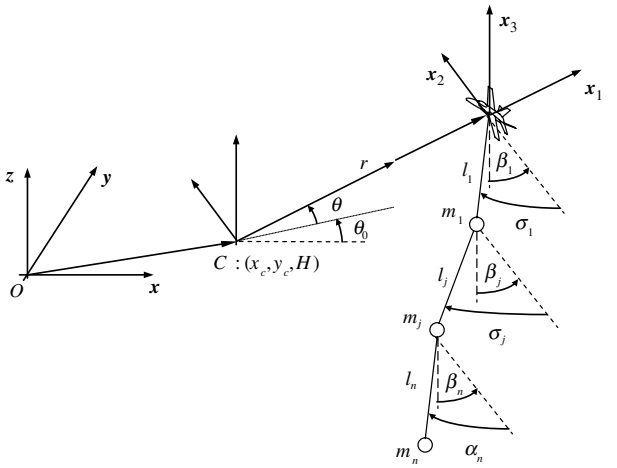

Fig. 1 Three-dimensional lumped mass model of an aerial-cable system.

The center of the aircraft orbit, denoted by C in Fig. 1, is considered static for each simulation run. Hence, we can consider C to be the center of the inertial coordinate frame for derivation of the equations of motion. In the following optimal control problem, it is desired to stabilize the cable tip at the point O in the presence of a crosswind. The position of the orbit center is used as an optimization parameter to shift the mean cable motion.

B. Equations of Motion

The positions of the point masses relative to the reference axes may be written in terms of the generalized coordinates as

$$\boldsymbol{r}_1 = (r - l_1 \sin\alpha_1)\boldsymbol{i} + (-l_1 \cos\alpha_1 \sin\beta_1)\boldsymbol{j} + (h - l_1 \cos\alpha_1 \cos\beta_1)\boldsymbol{k} \tag{1}$$

$$\boldsymbol{r}_j = \boldsymbol{r}_{j-1} - l_j \sin\alpha_j \boldsymbol{i} - l_j \cos\alpha_j \sin\beta_j \boldsymbol{j} - l_j \cos\alpha_j \cos\beta_j \boldsymbol{k}, \; j = 2, \ldots, n \tag{2}$$

The corresponding inertial velocities and accelerations are obtained by differentiating Eqs. (1) and (2). The results are given in Appendix A.

The goal for formulating the equations of motion in an efficient manner is to decouple the accelerations of mass j from all previous masses. This is accomplished by equating the accelerations with the specific forces on each mass, i.e.

$$\boldsymbol{a}_j = \frac{\boldsymbol{F}_j}{m_j} \tag{3}$$

The acceleration of mass j relative to mass $j-1$, $\boldsymbol{a}_{j|j-1}$, is obtained by subtracting subsequent accelerations, using Eq. (A4)

$$\boldsymbol{a}_{j|j-1} = \frac{\boldsymbol{F}_j}{m_j} - \frac{\boldsymbol{F}_{j-1}}{m_{j-1}} \tag{4}$$

The second derivatives of the generalized coordinates for each mass are obtained by transforming the accelerations from the orbital frame to the local tether frame (i.e., a frame with the $\boldsymbol{x}$ axis aligned with the tangent at segment j). The accelerations and forces are transformed from the rotational coordinate frame to the tether frame using the following direction cosine matrix

$$C_r^t = \begin{bmatrix} -\sin\alpha_j & -\cos\alpha_j \sin\beta_j & -\cos\alpha_j \cos\beta_j \\ -\cos\alpha_j & \sin\alpha_j \sin\beta_j & \sin\alpha_j \cos\beta_j \\ 0 & -\cos\beta_j & \sin\beta_j \end{bmatrix} \tag{5}$$

Multiplying both sides of Eq. (4) with this matrix leads to the decoupled equations

$$\begin{aligned} &\ddot{l}_1 - l_1\dot{\alpha}_1^2 - l_1\dot{\beta}_1^2\cos^2\alpha_1 - 2l_1\dot{\theta}\dot{\beta}_1 \sin\alpha_1 \cos\alpha_1 \cos\beta_1 \\ &\quad + \dot{\theta}^2 l_1 \cos^2\alpha_1 \cos^2\beta_1 - l_1\dot{\theta}^2 + 2l_1\dot{\theta}\dot{\alpha}_1 \sin\beta_1 + r\dot{\theta}^2 \sin\alpha_1 \\ &\quad - \ddot{h}\cos\alpha_1 \cos\beta_1 - r\ddot{\theta}\cos\alpha_1 \sin\beta_1 - 2\dot{r}\,\dot{\theta}\cos\alpha_1 \sin\beta_1 \\ &\quad - \ddot{r}\sin\alpha_1 = -\frac{F_1^x}{m_1}\sin\alpha_1 - \frac{F_1^y}{m_1}\cos\alpha_1 \sin\beta_1 - \frac{F_1^z}{m_1}\cos\alpha_1 \cos\beta_1 \end{aligned} \tag{6}$$

$$\begin{aligned} &l_1\ddot{\alpha}_1 - 2l_1\dot{\theta}\dot{\beta}_1\cos^2\alpha_1 \cos\beta_1 + l_1\dot{\beta}_1^2 \sin\alpha_1 \cos\alpha_1 - 2\dot{l}_1\dot{\theta}\sin\beta_1 \\ &\quad + 2\dot{l}_1\dot{\alpha}_1 - l_1\ddot{\theta}\sin\beta_1 - l_1\dot{\theta}^2\cos\alpha_1 \sin\alpha_1\cos^2\beta_1 \\ &\quad + \ddot{h}\sin\alpha_1 \cos\beta_1 + r\dot{\theta}^2\cos\alpha_1 - \ddot{r}\cos\alpha_1 + 2\dot{r}\,\dot{\theta}\sin\alpha_1 \sin\beta_1 \\ &\quad + r\ddot{\theta}\sin\alpha_1 \sin\beta_1 = -\left(\frac{F_1^x}{m_1}\right)\cos\alpha_1 + \left(\frac{F_1^y}{m_1}\right)\sin\alpha_1 \sin\beta_1 \\ &\quad + \left(\frac{F_1^z}{m_1}\right)\sin\alpha_1 \cos\beta_1 \end{aligned} \tag{7}$$

$$\begin{aligned} &l_1\ddot{\beta}_1 \cos\alpha_1 + l_1\ddot{\theta}\cos\beta_1 \sin\alpha_1 + 2\dot{l}_1\dot{\theta}\cos\beta_1 \sin\alpha_1 \\ &\quad + 2l_1\dot{\theta}\dot{\alpha}_1 \cos\beta_1 \cos\alpha_1 - l_1\dot{\theta}^2\cos\beta_1 \cos\alpha_1 \sin\beta_1 \\ &\quad + 2\dot{l}_1\dot{\beta}_1 \cos\alpha_1 - 2l_1\dot{\alpha}_1\dot{\beta}_1 \sin\alpha_1 - r\ddot{\theta}\cos\beta_1 - 2\dot{r}\,\dot{\theta}\cos\beta_1 \\ &\quad + \ddot{h}\sin\beta_1 = -\left(\frac{F_1^y}{m_1}\right)\cos\beta_1 + \left(\frac{F_1^z}{m_1}\right)\sin\beta_1 \end{aligned} \tag{8}$$

$$\begin{aligned} &\ddot{l}_j - l_j\dot{\alpha}_j^2 - l_j\dot{\beta}_j^2\cos^2\alpha_j - 2l_j\dot{\theta}\dot{\beta}_j \sin\alpha_j \cos\alpha_j \cos\beta_j \\ &\quad + \dot{\theta}^2 l_j \cos^2\alpha_j \cos^2\beta_j - l_j\dot{\theta}^2 + 2l_j\dot{\theta}\dot{\alpha}_j \sin\beta_j \\ &\quad = -\left(\frac{F_j^x}{m_j} - \frac{F_{j-1}^x}{m_{j-1}}\right)\sin\alpha_j - \left(\frac{F_j^y}{m_j} - \frac{F_{j-1}^y}{m_{j-1}}\right)\cos\alpha_j \sin\beta_j \\ &\quad - \left(\frac{F_j^z}{m_j} - \frac{F_{j-1}^z}{m_{j-1}}\right)\cos\alpha_j \cos\beta_j \end{aligned} \tag{9}$$

$$\begin{aligned} &l_j\ddot{\alpha}_j - 2l_j\dot{\theta}\dot{\beta}_j\cos^2\alpha_j \cos\beta_j + l_j\dot{\beta}_j^2 \sin\alpha_j \cos\alpha_j - 2\dot{l}_j\dot{\theta}\sin\beta_j \\ &\quad + 2\dot{l}_j\dot{\alpha}_j - l_j\ddot{\theta}\sin\beta_j - l_j\dot{\theta}^2\cos\alpha_j \sin\alpha_j\cos^2\beta_j \\ &\quad = -\left(\frac{F_j^x}{m_j} - \frac{F_{j-1}^x}{m_{j-1}}\right)\cos\alpha_j + \left(\frac{F_j^y}{m_j} - \frac{F_{j-1}^y}{m_{j-1}}\right)\sin\alpha_j \sin\beta_j \\ &\quad + \left(\frac{F_j^z}{m_j} - \frac{F_{j-1}^z}{m_{j-1}}\right)\sin\alpha_j \cos\beta_j \end{aligned} \tag{10}$$

$$\begin{aligned} &l_j\ddot{\beta}_j \cos\alpha_j + l_j\ddot{\theta}\cos\beta_j \sin\alpha_j + 2\dot{l}_j\dot{\theta}\cos\beta_j \sin\alpha_j \\ &\quad + 2l_j\dot{\theta}\dot{\alpha}_j \cos\beta_j \cos\alpha_j - l_j\dot{\theta}^2\cos\beta_j \cos\alpha_j \sin\beta_j \\ &\quad + 2\dot{l}_j\dot{\beta}_j \cos\alpha_j - 2l_j\dot{\alpha}_j\dot{\beta}_j \sin\alpha_j \\ &\quad = -\left(\frac{F_j^y}{m_j} - \frac{F_{j-1}^y}{m_{j-1}}\right)\cos\beta_j + \left(\frac{F_j^z}{m_j} - \frac{F_{j-1}^z}{m_{j-1}}\right)\sin\beta_j \end{aligned} \tag{11}$$

If the tether is modeled as elastic, then the second derivatives of the generalized coordinates can be obtained simply from Eqs. (6–11). However, modeling the links as elastic introduces high-frequency longitudinal oscillations that makes numerical analysis difficult. Instead, the tether is treated as inelastic which means that it is first necessary to determine the distribution of tension throughout the cable so that the equations of motion for the accelerations can be determined.

C. Tension Distribution

Assume that all external forces on the lumped masses are known at any instant of time. The tension forces are always directed along the tether segment. Hence, the sum of the tension forces on the jth lumped mass can be written as

$$\begin{aligned} \boldsymbol{F}_j^t &= (T_j \sin\alpha_j - T_{j+1}\sin\alpha_{j+1})\boldsymbol{i} + (T_j \cos\alpha_j \sin\beta_j \\ &\quad - T_{j+1}\cos\alpha_{j+1}\sin\beta_{j+1})\boldsymbol{j} + (T_j \cos\alpha_j \cos\beta_j \\ &\quad - T_{j+1}\cos\alpha_{j+1}\cos\beta_{j+1})\boldsymbol{k} \end{aligned} \tag{12}$$

The assumption is made that the variation in the segment lengths is either fixed, or prescribed as a function of time via $\ddot{l}_1$. Substitution of Eq. (12) into Eqs. (6) and (9) results in a system of linear equations for the n tension values. Solving the system of equations gives the tensions in all the segments, which can be used to evaluate the angular accelerations of the tether segments. The constraint equations are given in Appendix B. Note that the tension forces depend on the orbital motion of the aircraft, and all other external forces acting on the cable and towed body. Simulations can be carried out easily for elastic cables by substituting the tension distribution with one obtained using a constitutive law.

D. Force Equations

1. *Aerodynamic Drag*

The aerodynamic drag acting on the cable is determined via a crossflow model. The aerodynamic lift and drag coefficients are defined as functions of the segment angle of attack, ϑ_j. The corresponding lift and drag forces are calculated using the velocity of the cable segment relative to the wind. This may be approximated from the motion of the adjacent masses as

$$\boldsymbol{v}_j^{\text{rel}} = \boldsymbol{v}_j - \boldsymbol{v}_j^{\text{wind}} = v_{x_j}^{\text{rel}}\boldsymbol{i} + \boldsymbol{v}_{y_j}^{\text{rel}}\boldsymbol{j} + \boldsymbol{v}_{z_j}^{\text{rel}}\boldsymbol{k} \tag{13}$$

The lift and drag coefficients for an inclined circular cylinder are given by [23]

$$C_{D_j} = C_{D_f} + C_{D_{\text{basic}}}\sin^3\vartheta_j \approx 0.022 + 1.1\sin^3\vartheta_j \tag{14}$$

$$C_{L_j} = C_{D_{\text{basic}}}\sin^2\vartheta_j \cos\vartheta_j \approx 1.1\sin^2\vartheta_j \cos\vartheta_j \tag{15}$$

It has been assumed that the flow around the cable is subsonic. For higher Reynold's numbers, or in the presence of vortex shedding, more complex models of the aerodynamic force coefficients will be required.

The angle of attack may be calculated from

$$\begin{aligned} \cos\vartheta_j &= \frac{-\boldsymbol{l}_j \cdot \boldsymbol{v}_j^{\text{rel}}}{|\boldsymbol{l}_j||\boldsymbol{v}_j^{\text{rel}}|} \\ &= \frac{v_{x_j}^{\text{rel}}\sin\alpha_j + v_{y_j}^{\text{rel}}\cos\alpha_j \sin\beta_j + v_{z_j}^{\text{rel}}\cos\alpha_j \cos\beta_j}{\sqrt{(v_{x_j}^{\text{rel}})^2 + (v_{y_j}^{\text{rel}})^2 + (v_{z_j}^{\text{rel}})^2}} \end{aligned} \tag{16}$$

where

$$\boldsymbol{l}_j = -l_j \sin\alpha_j\boldsymbol{i} - l_j\cos\alpha_j \sin\beta_j\boldsymbol{j} - l_j\cos\alpha_j \cos\beta_j\boldsymbol{k} \tag{17}$$

The unit vectors defining the directions of the lift and drag vectors are

$$\boldsymbol{e}_D = -\frac{\boldsymbol{v}_j^{\text{rel}}}{|\boldsymbol{v}_j^{\text{rel}}|} \tag{18}$$

$$\boldsymbol{e}_L = -\frac{(\boldsymbol{v}_j^{\text{rel}} \times \boldsymbol{l}_j) \times \boldsymbol{v}_j^{\text{rel}}}{|(\boldsymbol{v}_j^{\text{rel}} \times \boldsymbol{l}_j) \times \boldsymbol{v}_j^{\text{rel}}|} = \frac{e_x \boldsymbol{i} + e_y \boldsymbol{j} + e_z \boldsymbol{k}}{\sqrt{e_x^2 + e_y^2 + e_z^2}} \tag{19}$$

where

$$\begin{aligned} e_x = {} & (v_{z_j}^{\text{rel}})^2 \sin\alpha_j - v_{z_j}^{\text{rel}} v_{x_j}^{\text{rel}} \cos\alpha_j \cos\beta_j \\ & - v_{y_j}^{\text{rel}} v_{x_j}^{\text{rel}} \cos\alpha_j \sin\beta_j + (v_{y_j}^{\text{rel}})^2 \sin\alpha_j \end{aligned} \tag{20}$$

$$\begin{aligned} e_y = {} & (v_{x_j}^{\text{rel}})^2 \cos\alpha_j \sin\beta_j - v_{x_j}^{\text{rel}} v_{y_j}^{\text{rel}} \sin\alpha_j \\ & - v_{y_j}^{\text{rel}} v_{z_j}^{\text{rel}} \cos\alpha_j \cos\beta_j + (v_{z_j}^{\text{rel}})^2 \cos\alpha_j \sin\beta_j \end{aligned} \tag{21}$$

$$\begin{aligned} e_z = {} & (v_{y_j}^{\text{rel}})^2 \cos\alpha_j \cos\beta_j - v_{y_j}^{\text{rel}} v_{z_j}^{\text{rel}} \cos\alpha_j \sin\beta_j \\ & - v_{x_j}^{\text{rel}} v_{z_j}^{\text{rel}} \sin\alpha_j + (v_{x_j}^{\text{rel}})^2 \cos\alpha_j \cos\beta_j \end{aligned} \tag{22}$$

Hence, the lift and drag vectors may be written as

$$\boldsymbol{F}_j^{\text{drag}} = \frac{1}{2} \rho C_{D_j} l_j d |\boldsymbol{v}_j^c|^2 \boldsymbol{e}_D \tag{23}$$

$$\boldsymbol{F}_j^{\text{lift}} = \frac{1}{2} \rho C_{L_j} l_j d |\boldsymbol{v}_j^c|^2 \boldsymbol{e}_L \tag{24}$$

These lift and drag vectors are assumed to be constant over each cable segment. Hence the aerodynamic forces are lumped to each point mass taking half from each adjacent segment,

$$\boldsymbol{F}_j^{\text{aero}} = \boldsymbol{F}_j^{\text{drag}} + \boldsymbol{F}_j^{\text{lift}} \tag{25}$$

The towed vehicle is assumed to be spherical, generating drag only.

2. Gravity Forces

The gravity forces are assumed to be due to a flat Earth and are assumed invariant with altitude

$$\boldsymbol{F}_j^{g} = -m_j g \boldsymbol{k} \tag{26}$$

3. Model Validation

The modeling approach used above has been compared with existing experimental data and the results are presented in [24]. In general, very good agreement is achieved between the model and experimental data, provided the angular velocity of the tether system at the towpoint is low. This is true of the configurations studied in this work.

III. Aircraft Motion Model

The motion of the towpoint, together with the cable properties, defines the physical motion of the system. In this paper, the towpoint is assumed to be an aircraft. Hence, there is a range of motion of the towpoint that is applicable to a particular aircraft, and others that are not. The aim of this section is to develop a parameterization of the aircraft motion that can be used for optimization. Because most aircraft autopilots are designed to fly at constant airspeed, the motion model is developed so that the towpoint maintains a constant speed relative to the air mass. The air mass is assumed to move at a constant speed relative to the ground, and in a constant direction.

A. Orbital Angular Velocity

Consider the motion of the aircraft prescribed to follow an elliptical orbit in the horizontal plane. The orbit may be parameterized by the semimajor axis a, and eccentricity e,

$$r = \frac{a(1-e^2)}{1 + e\cos\theta} \triangleq \frac{p}{\kappa} \tag{27}$$

The rate of change of the orbit radius with respect to time is given by

$$\dot{r} = \frac{ep\dot{\theta}\sin\theta}{\kappa^2} \tag{28}$$

At this point, the angular velocity of the aircraft in the horizontal plane is unknown. It is the goal of this section to derive an analytic expression for the angular velocity that maintains constant airspeed in an elliptical orbit. For generality, a vertical periodic component is also added to the aircraft motion of the form

$$\Delta h = h_d \sin(\theta + \theta_h) \tag{29}$$

which is superimposed onto the mean aircraft altitude. The phase θ_h allows the plane of the orbit relative to the wind direction to be rotated. For simplicity, the wind direction is assumed to be parallel to the inertial $\boldsymbol{x}$ axis. The wind speed can be expressed in the rotational frame attached to the aircraft as

$$\boldsymbol{v}_w^{\text{rot}} = V_w \cos(\theta + \theta_0)\boldsymbol{i} - V_w \sin(\theta + \theta_0)\boldsymbol{j} \tag{30}$$

where θ_0 is used to rotate the elliptical orbit relative to the wind direction. The total airspeed of the aircraft may be expressed as

$$V_a = \sqrt{(\dot{r} - \boldsymbol{v}_w^{\text{rot}} \cdot \boldsymbol{i})^2 + (r\dot{\theta} - \boldsymbol{v}_w^{\text{rot}} \cdot \boldsymbol{i})^2 + \dot{h}^2} \tag{31}$$

Equating the airspeed to a fixed quantity, V_T, and squaring both sides leads to a quadratic equation for $\dot{\theta}$

$$\begin{aligned} & \left[\left(\frac{ep}{\kappa^2}\sin\theta\right)^2 + \left(\frac{p}{\kappa}\right)^2 + h_d^2 \cos^2(\theta + \theta_h)\right]\dot{\theta}^2 \\ & \quad + \left[2\frac{p}{\kappa} V_w \sin(\theta + \theta_0) - 2\frac{ep}{\kappa^2} V_w \sin\theta\cos(\theta + \theta_0)\right]\dot{\theta} \\ & \quad + [V_w^2 - V_T^2] = 0 \end{aligned} \tag{32}$$

The solution of this equation for $\dot{\theta}$ must be positive, which means that the positive root must be taken,

$$\begin{aligned} \dot{\theta} = {} & -\frac{[\frac{p}{\kappa} V_w \sin(\theta + \theta_0) - \frac{ep}{\kappa^2} V_w \sin\theta\cos(\theta + \theta_0)]}{[(\frac{ep}{\kappa^2}\sin\theta)^2 + (\frac{p}{\kappa})^2 + h_d^2\cos^2(\theta + \theta_h)]} \\ & + \frac{([2\frac{p}{\kappa} V_w \sin(\theta + \theta_0) - 2\frac{ep}{\kappa^2} V_w \sin\theta\cos(\theta + \theta_0)]^2 - 4[(\frac{ep}{\kappa^2}\sin\theta)^2 + (\frac{p}{\kappa})^2 + h_d^2\cos^2(\theta + \theta_h)][V_w^2 - V_T^2])^{1/2}}{2[(\frac{ep}{\kappa^2}\sin\theta)^2 + (\frac{p}{\kappa})^2 + h_d^2\cos^2(\theta + \theta_h)]} \end{aligned} \tag{33}$$

For the case of no wind, the following simplified expression can be obtained

$$\dot{\theta} = \frac{V_T([(\frac{ep}{\kappa^2}\sin\theta)^2 + (\frac{p}{\kappa})^2 + h_d^2\cos^2(\theta + \theta_h)])^{1/2}}{[(\frac{ep}{\kappa^2}\sin\theta)^2 + (\frac{p}{\kappa})^2 + h_d^2\cos^2(\theta + \theta_h)]} \tag{34}$$

For the case of a circular orbit in the horizontal plane, the angular velocity reduces to

$$\dot{\theta} = -\frac{V_w \sin(\theta + \theta_0)}{R} + \frac{\sqrt{V_w^2 \sin^2(\theta + \theta_0) + V_T^2 - V_w^2}}{R} \tag{35}$$

It is readily verified that the angular velocity reduces to that of a standard circular orbit when the wind speed is zero. Furthermore, Eq. (35) shows that the tangential velocity of the aircraft is equal to $V_T - V_w$ when it is flying into the wind direction, and is $V_T + V_w$ when flying downwind.

B. Orbit Period

The time taken to complete one orbital revolution, T_p, is calculated from Eq. (33) using numerical integration as follows

$$T_p = \int_0^{2\pi} \frac{1}{\dot{\theta}} \, \mathrm{d}\theta \tag{36}$$

An adaptive Simpson rule is used to evaluate this integral to double precision.

C. Variation in Length

For the case where the cable length is allowed to be varied, it is done so in a periodic manner similar to the variation in aircraft altitude

$$\Delta L = \frac{L_d}{2}\left[1 + \sin\left(\theta + \frac{3\pi}{2} + \theta_L\right)\right] \tag{37}$$

where L_d is the maximum amount of additional cable that is deployed, and θ_L is used to phase the variation in length with respect to the wind.

D. Position of Cable Tip

The position of the cable tip in the inertial frame can be computed assuming an offset in the orbit center of (x_c, y_c, H),

$$\begin{aligned} x_{\text{tip}} &= x_c + \left(r - \sum_{j=1}^{n} l_j \sin\alpha_j\right)\cos(\theta + \theta_0) \\ &\quad - \left(-\sum_{j=1}^{n} l_j \cos\alpha_j \sin\beta_j\right)\sin(\theta + \theta_0) \\ y_{\text{tip}} &= y_c + \left(r - \sum_{j=1}^{n} l_j \sin\alpha_j\right)\sin(\theta + \theta_0) \\ &\quad + \left(-\sum_{j=1}^{n} l_j \cos\alpha_j \sin\beta_j\right)\cos(\theta + \theta_0) \\ z_{\text{tip}} &= H - \sum_{j=1}^{n} l_j \cos\alpha_j \cos\beta_j \end{aligned} \tag{38}$$

IV. Numerical Analysis of Cable Motion

In this section, periodic solutions of the towed cable system are generated for different towpoint conditions and environmental conditions. Periodic solutions for the towed cable system are generated using a Newton algorithm with derivatives generated via finite differences. For the range of motion and force models considered in this paper, the cable takes on only one stable equilibrium position. The search algorithm commences at the steady-state, stationary solution for the cable with the towpoint in a circular orbit, and with zero crosswind. Each parameter is varied separately using a homotopy approach. Because the periodic solutions are stable, the Newton algorithm converges very quickly to a solution.

A. Initial Guess Generation

The initial guess used for the homotopy approach is the relative equilibrium position. Such stationary configurations have been studied at length in other works. In this paper, the shooting method given in [16] is used to obtain the stationary configuration of the cable. The basic method is summarized here for convenience.

1) The orbit radius r and speed V_T of the aircraft are specified.

2) A cable length L, degree of cable discretization n, and length distribution are specified.

3) An initial guess of the towed body radius in the rotational frame is given, r_t. The position is arbitrarily selected to lie on the $\boldsymbol{x}$ axis in the orbital frame.

4) The sum of forces due to drag, gravity, and inertial forces are used to establish the tension force on the towed body.

5) The tension force vector is used to establish a unit vector from the towed body to the next lumped mass, m_{n-1}.

6) The length of element n, l_n, is used to establish the position of mass m_{n-1}.

7) The position of the lumped mass allows calculation of drag forces, inertial forces, and gravity forces.

8) The unknown tension vector is calculated, and steps 5–7 are repeated until the end of the cable is reached.

9) The difference in orbit radius of the end of the cable and the desired orbit radius r for the aircraft is driven to zero using r_t as the decision variable.

10) The positions of the aircraft and cable in the rotational frame are rotated so that the aircraft lies on the $\boldsymbol{x}$ axis of the rotational frame.

B. Periodic Solution Generation

By definition, a periodic solution has zero net energy gained or lost during one orbit. The stationary configuration is itself a periodic solution with period $2\pi r/V_T$. Denote the initial stationary solution as $\boldsymbol{x}_0$. Assume that the perturbation parameter is denoted by p, with homotopy step Δp. The initial conditions of the perturbed solution are computed using Newton's method applied to

$$\boldsymbol{F} = \int_{t_0}^{T_p} \dot{\boldsymbol{x}} \, \mathrm{d}t - \boldsymbol{x}_0(p + \Delta p) = \boldsymbol{0} \tag{39}$$

where the initial condition for evaluation of the integral is $\boldsymbol{x}_0(p + \Delta p)$. The Jacobian matrix of Eq. (39), $\partial \boldsymbol{F}/\partial \boldsymbol{x}_0$ is approximated via finite differences.

C. Effect of Number of Masses

In this section, the effect of the degree of discretization of the cable is assessed. This is important because it is highly desirable to minimize the number of elements used in the model for the sake of computational efficiency. It has been found that best accuracy can be achieved by using an uneven distribution of masses/segment lengths. This is due to the fact that the portion of the cable closest to the aircraft is subjected to higher drag than the tip of the cable. Hence, it

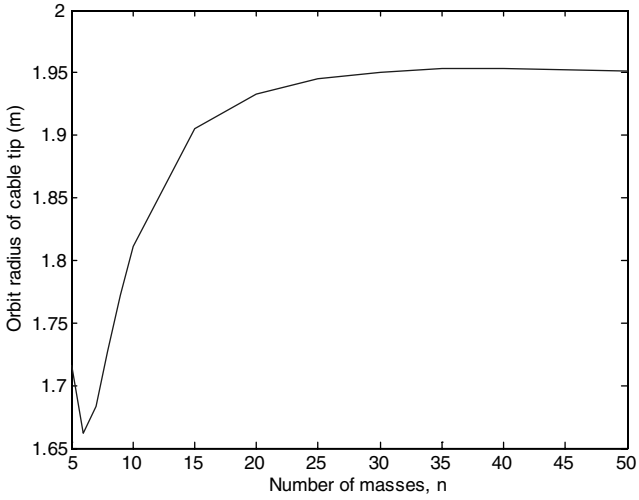

Fig. 2 Convergence of steady-state orbit radius of cable tip with number of elements.

Table 1 Nominal aircraft/cable properties

Parameter	Value
Cable length	2500 m
Cable diameter	2 mm
Cable mass density	1040 kg/m^3
Aircraft speed	60 m/s
Aircraft orbit radius	250 m
End body mass	10 kg
End body drag, C_DA	2 m^2

is desirable to have a higher fidelity cable representation in the upper cable rather than in the lower one. For this reason, the cable segment lengths are distributed in a logarithmic manner with the shortest elements closest to the aircraft.

Figure 2 shows the orbit radius of the cable tip derived from the model as a function of number of cable elements for the system properties shown in Table 1. This shows that with logarithmically spaced elements the solution can be reasonably well approximated with even a handful of masses. For the remainder of this paper, 10 cable elements are used to provide a good compromise between computational expense and accuracy. Figure 3 shows a three-dimensional plot of the cable shape derived for different numbers of elements. This shows that even with 5 masses the cable shape is close to that derived for the cable shape using 50 masses.

D. Numerical Results for Effect of Orbital Parameters on Cable Response

1. *Effect of Crosswind*

The effect of crosswind was determined by varying the wind speed in the ***x*** direction from 0 to 5 m/s, with the system parameters given in Table 1. The periodic motion of the cable tip in the inertial frame is shown in Fig. 4. The main effect of the crosswind is to shift the position of the cable tip downwind. In fact, the results show this to be a very significant shift for a 5 m/s crosswind. The resulting mean position of the cable tip is over 1200 m downwind. The second major effect of the crosswind is that it causes the cable tip to oscillate in the vertical plane. For the case of a 5 m/s crosswind, the peak-to-peak oscillation magnitude is approximately 70 m. A close-up of the periodic solution for a 5 m/s crosswind is shown in Fig. 5. This plot shows that the variation of the orbit of the cable tip in the ***y*** direction (normal to the wind direction) is very small in comparison to the vertical oscillation. The third effect of the crosswind is that the cable tip is pulled in a direction which is normal to the wind direction. The movement is positive in the direction of the angular velocity vector of the aircraft. This relative effect of this is second-order compared with the movement of the cable tip due to drag. Figure 6 shows the cable shape for the case of a 5 m/s crosswind. This shows that the cable undergoes a compressive effect when the aircraft is flying towards the cable tip, and an expansion effect when the aircraft is flying away from the cable tip. This causes a change in the cable tension, resulting in the height of the cable tip to vary. These results clearly indicate that a crosswind is a significant disturbance that would need to be compensated for during accurate positioning of the cable tip. These results also give some insight into how the effect of wind can be compensated for. One possibility is to shift the center of the aircraft orbit in conjunction with either tether reeling or varying the height of the aircraft to compensate for the variation in height. However, the effects of tether reeling or varying the aircraft altitude need to be assessed.

2. *Effect of Elliptical Orbit*

The effect of flying the aircraft in an elliptical orbit was assessed by varying the eccentricity from 0 to 0.8 while maintaining the semimajor axis at 250 m. All other system parameters are given in Table 1. The results, shown in Fig. 7, illustrate that the main effect of the eccentricity is a shift in the mean motion of the cable tip towards the geometric center of the ellipse. Since the origin of the coordinate

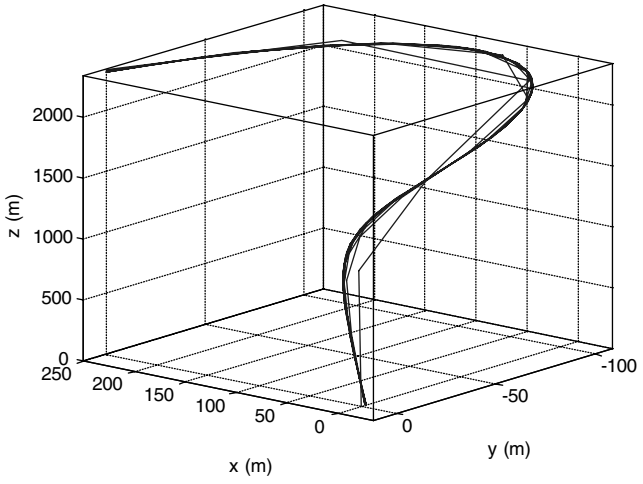

Fig. 3 Cable shape for circular aircraft orbit, shown for different numbers of cable elements (5 though 50).

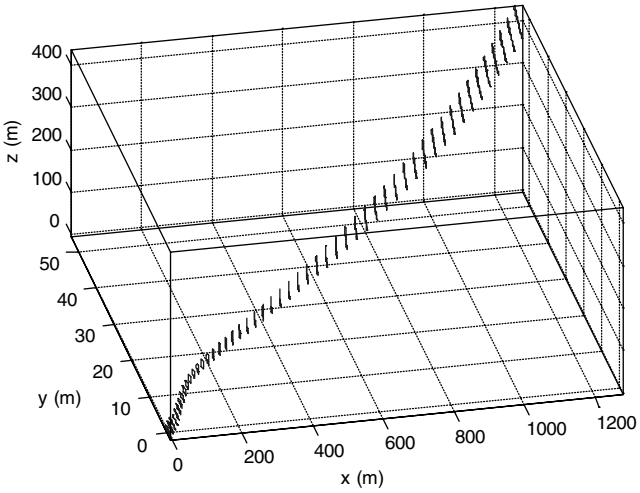

Fig. 4 Effect of crosswind (0–5 m/s) on periodic solution of cable tip, shown in inertial frame.

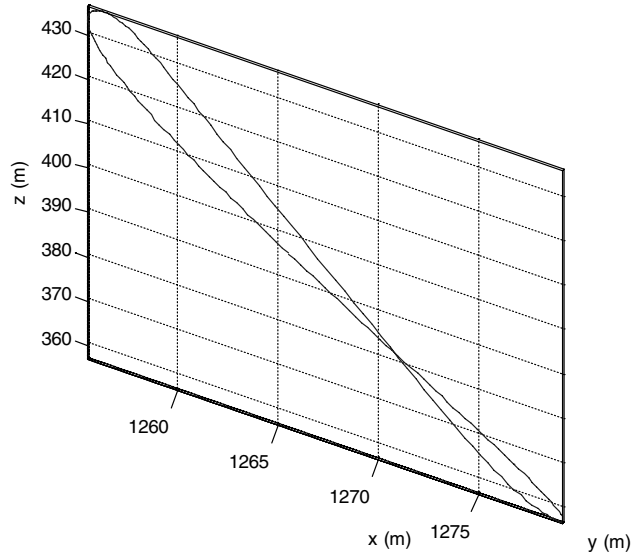

Fig. 5 Effect of 5 m/s crosswind on periodic solution of cable tip.

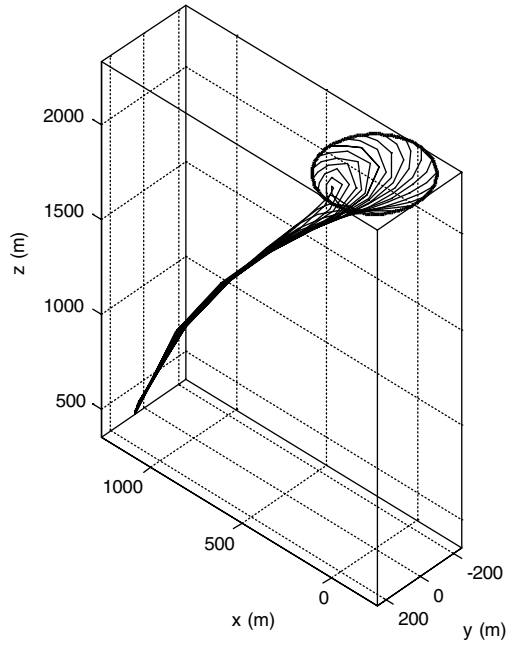

Fig. 6 Effect of 5 m/s crosswind on periodic solution of cable shape.

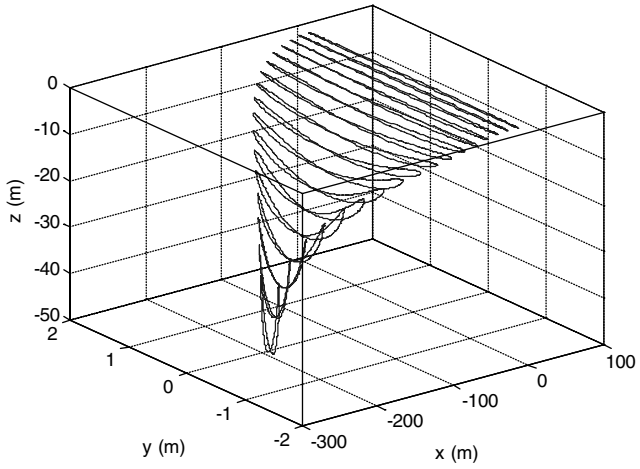

Fig. 7 Effect of elliptical orbit on periodic solution of cable tip ($0 \le e \le 0.8$, in steps of 0.05).

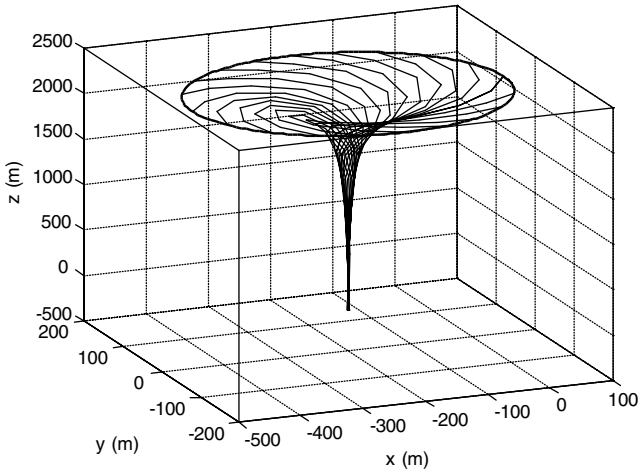

Fig. 8 Motion of cable during periodic solution with orbit eccentricity 0.8.

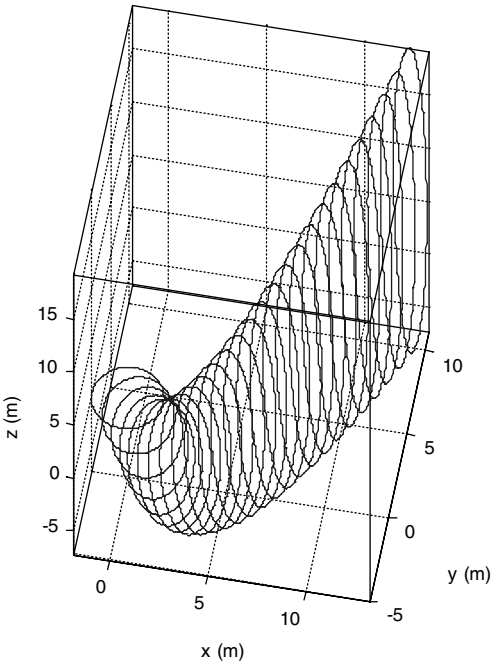

Fig. 9 Effect of sinusoidal variation in aircraft height on cable tip response ($h_d = 0$ to 50 m).

system remains fixed at the focus of the ellipse, it is evident that the cable tip remains closest to the center of the motion and not the focus of the ellipse. This is caused by the constraint on the airspeed of the aircraft to remain constant. The second effect of the elliptical orbit is a drop in altitude of the cable tip, combined with a small vertical oscillation. The amplitude of the vertical oscillation is on the order of 10 m, whereas the drop in altitude is on the order of 40 m for an eccentricity of 0.8. Figure 8 shows the motion of the cable for the cable of $e = 0.8$. This clearly shows that the cable is concentrated at the geometric center of the ellipse.

3. *Effect of Height Variation*

The effect of flying the aircraft in an inclined orbit was assessed by varying h_d from 0 to 50 m, with $\theta_h = 0$. All other system parameters are given in Table 1. The resulting periodic solutions of the cable tip are shown in Fig. 9. This shows that the primary effect of varying the aircraft height is that the cable tip oscillates in a circular orbit in the vertical plane. For the case of a vertical oscillation amplitude of 50 m, the cable tip peak-to-peak oscillation is 26.5 m. The induced vertical motion also causes the cable tip to move away from the origin in the horizontal plane. The movement is on the order of 10 m in the x and y directions for a height variation of 50 m.

4. *Effect of Length Variation*

The effect of varying the cable length on the cable tip response was assessed by varying L_d from 0 to 200 m. The system parameters remain the same as those shown in Table 1. The periodic solutions of the cable tip are shown in Fig. 10. A close-up of the cable tip motion for a 200 m variation in cable length is shown in Fig. 11. The results show that the variation in cable length has a similar effect on the cable tip motion as a variation in altitude of the aircraft. The main effect is a variation in altitude of the tip. The effect is less severe than varying the aircraft altitude. For example, for a length variation of 50 m, the peak-to-peak oscillation of the cable tip is 16.3 m, compared with 26.5 m when a direct height variation of the aircraft is used. The difference is due to the fact that the cable is not completely vertical. In other words, deployment of the cable results in components of the length increasing in the horizontal plane. The results also show that as the variation in length increases, the cable tip moves away from the orbit center.

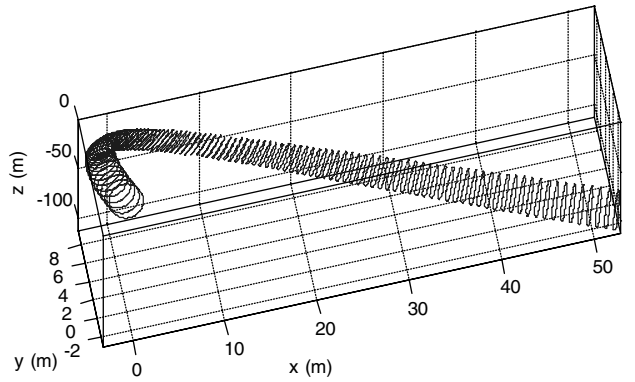

Fig. 10 Effect of sinusoidal variation in cable length ($L_d = 0$ to 200 m amplitude).

V. Optimization of Towed System

A. Problem Statement

The aerial-cable system represents a complex system with many state variables and dynamic vibration modes. One possible way of determining the optimal means for flying the aircraft to minimize the effects of crosswind on the cable tip response is to formulate the full optimal control problem involving the equations of motion for the cable elements. In such a formulation, the second derivatives of the orbit radius, $\ddot{r}$, and orbit angle, $\ddot{\theta}$, as well as the second derivative or cable length, $\ddot{l}_1$, or aircraft altitude, $\ddot{h}$, could be used as pseudocontrol inputs. In [22], this approach was used in combination with direct transcription. Direct transcription approximates the differential equations by means of equality constraints in a nonlinear programming problem. However, this results in a very large scale nonlinear programming due to the high number of collocation points needed to adequately capture the cable response. Instead of taking this approach, an alternative formulation is used in this paper.

The problem is posed as follows: find the optimal design vector $\boldsymbol{p} := (\boldsymbol{x}_0, a, e, V_T, \theta_0, h_d, \theta_h, H, x_c, y_c, L_d, \theta_L)$ to minimize the cost function

$$J = \int_0^{T_p} (x_{\text{tip}}^2 + y_{\text{tip}}^2 + h_{\text{tip}}^2)\, \mathrm{d}t \tag{40}$$

Subject to the equations of motion defined in Sec. II, the periodicity constraints

$$\boldsymbol{x}_0 - \boldsymbol{x}(T_p) = \boldsymbol{0} \tag{41}$$

as well as box constraints on the design vector

$$\boldsymbol{p}_L \le \boldsymbol{p} \le \boldsymbol{p}_U \tag{42}$$

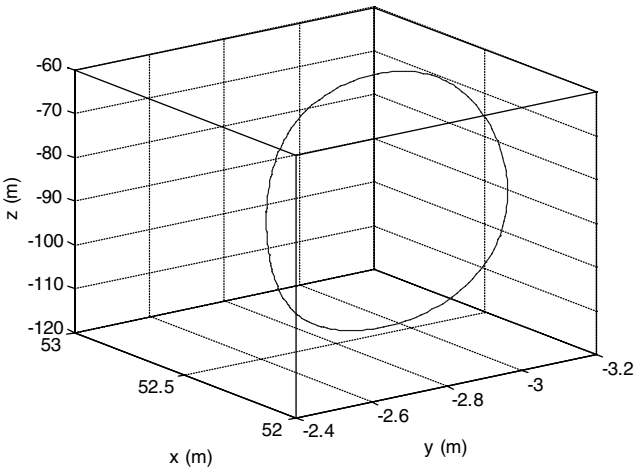

Fig. 11 Effect of 200 m variation in cable length on cable tip response.

The method for solving this problem is outlined in the following subsection.

B. Solution Method

The number of differential equations that are needed to simulate the cable dynamics is $4n$, where n is the number of elements. An additional differential equation is needed for integrating the angular position of the aircraft. Hence, even with the cable modeled using 10 elements, 41 differential equations need to be propagated or transcribed. Instead of using direct transcription, which approximates the solution of differential equations by using a set of nonlinear algebraic equations that are driven to zero by nonlinear programming software, the equations of motion are propagated directly using a fourth-order Runge–Kutta method with a fixed time step. The equations of motion are integrated from the start time to the final time in one pass. Iterating on the decision variables in this manner is often referred to as direct shooting. Direct multiple shooting can be used in problems with a high sensitivity of the differential equations to the decision vector. Direct multiple shooting divides the entire time interval of interest into several subintervals with equality constraints applied on the states across the intervals. This is done to desensitize the variation in states to changes in initial conditions. However, for the towed cable system, since the motion is stabilized by aerodynamic drag, the differential equations remain stable when propagated. Hence, there is no need to use direct multiple shooting or direct transcription to solve the differential equations in the optimization problem.

The equations of motion are propagated using a C++ mex-file interface in MATLAB. A Gaussian elimination routine from LAPACK is used to solve the tension equations. The optimization problem is solved using the software SNOPT [25], also compiled with a mex-file interface.

VI. Numerical Results

Optimization of the aircraft motion to compensate for the effects of a crosswind was approached using two different methods. In the first method, the aircraft altitude was held fixed, and the length of cable was varied to stabilize the vertical motion of the cable tip. In the second method, the cable length was held fixed, and the aircraft altitude was varied.

A. Aircraft Altitude Fixed

Optimal results were obtained for crosswinds of 0 to 5 m/s in steps of 0.05 m/s. The optimal aircraft orbit is shown in Fig. 12 as a function of wind speed. Based on the results obtained above, it is clear that the major compensation for the crosswind is a shift in the aircraft orbit. The orbit is shifted upwind, with a smaller shift perpendicular to the wind direction. Figure 13 shows the compensated motion of the cable tip trajectory in the horizontal plane. This shows that the compensated motion in the horizontal plane results in smaller orbit radii than the unperturbed circular orbit. Figure 14 shows the compensated three-dimensional trajectory of the cable tip. This illustrates that the vertical motion becomes the dominant effect on the motion for high wind speeds. However, even for wind speeds

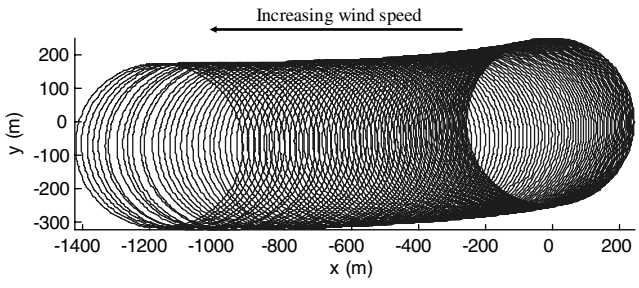

Fig. 12 Optimal aircraft orbit to compensate for crosswind in $+x$ direction.

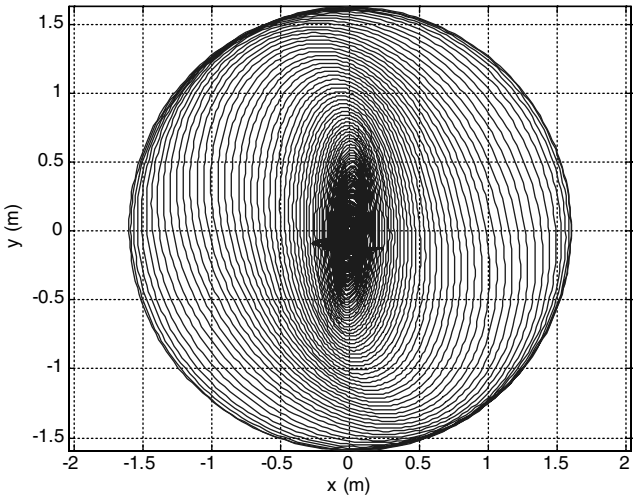

Fig. 13 Compensated projection of the orbit of cable tip in inertial frame, shown in the horizontal plane (wind speed from 0 to 5 m/s).

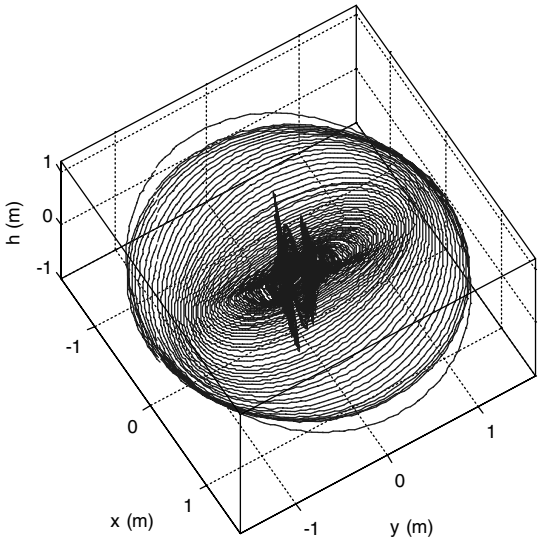

Fig. 14 Compensated orbit of cable tip in inertial frame (wind speed from 0 to 5 m/s).

of 5 m/s, the error in vertical position is on the order of 1 m, which is smaller than the unperturbed orbit radius of the tip (1.66 m).

Figure 15 shows the optimal shift in aircraft orbit as a function of wind speed, and Fig. 16 and 17 shows the orbital parameters of the aircraft. The results show that the aircraft is flown in an elliptic orbit with the eccentricity increasing with the wind speed. The orbit altitude initially increases with wind speed until approximately 3 m/s, then decreases rapidly with wind speed. The semimajor axis is generally constant with wind speed, except for wind speeds above 3 m/s, where there appears to be some noise in the results. Figure 18 shows the variation in cable length and phasing of the reeling relative to the periapsis of the ellipse. To compensate for the vertical motion of the cable tip, the cable must be reeled at increasing speeds.

B. Fixed Cable Length

The alternative to reeling the cable is varying the altitude of the aircraft. Figure 19 shows the optimal aircraft orbit in the horizontal plane for crosswind speeds of 0 to 5 m/s. Unlike the case where reeling is used, the shift in the aircraft orbit is predominantly in the upwind direction with very little shift perpendicular to the wind direction. Figure 20 shows the trajectory of the cable tip in the

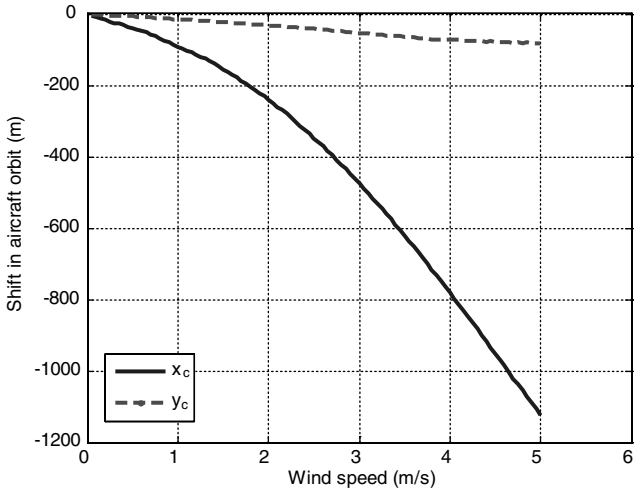

Fig. 15 Shift in aircraft orbit as a function of wind speed.

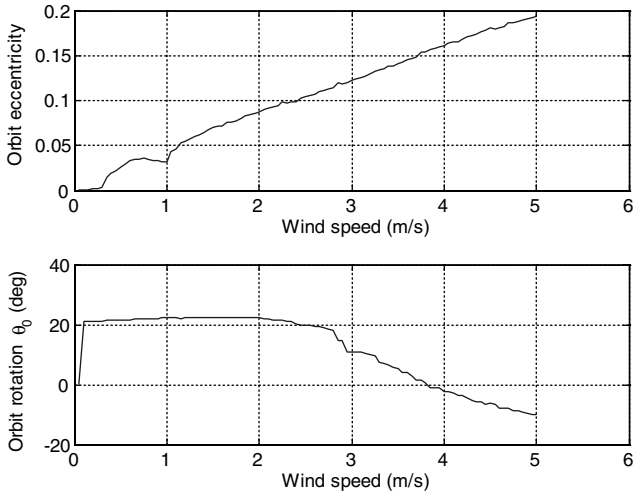

Fig. 16 Optimal orbit eccentricity and orientation of major axis of ellipse for compensating for effect of crosswind.

horizontal plane. For wind speeds between 0 and 2 m/s, the trajectories match those of the cable reeling solutions reasonably well. However, above 2 m/s, the trajectories are disturbed from their positions centered at the origin with large excursions in the

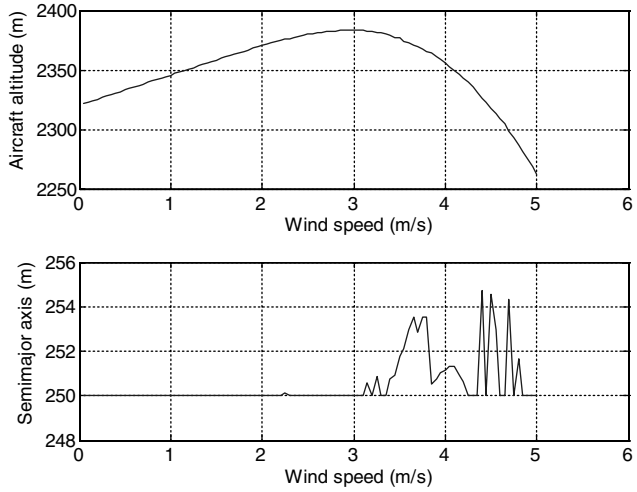

Fig. 17 Optimal aircraft altitude and semimajor axis for compensating for effect of crosswind.

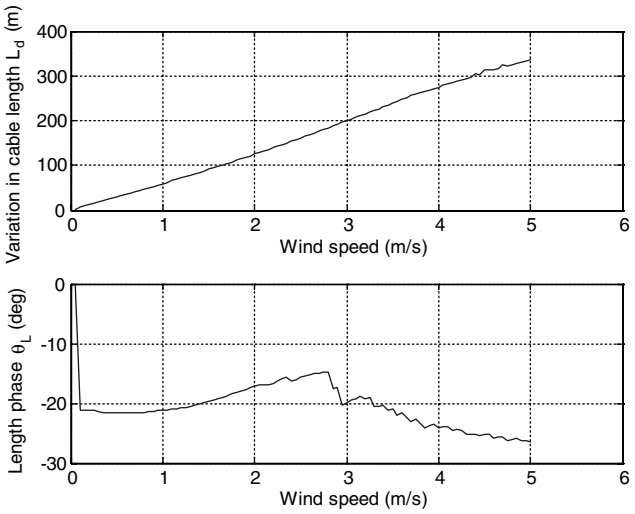

Fig. 18 Optimal variation and phasing of length to compensate for effects of cross wind.

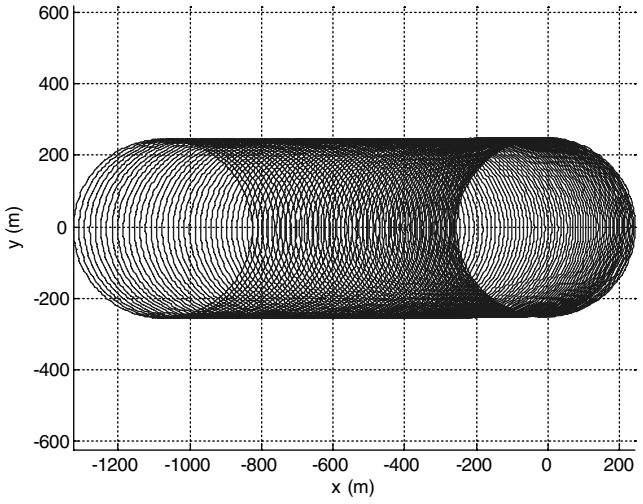

Fig. 19 Optimal aircraft orbit to compensate for crosswind in $+x$ direction, with cable length fixed.

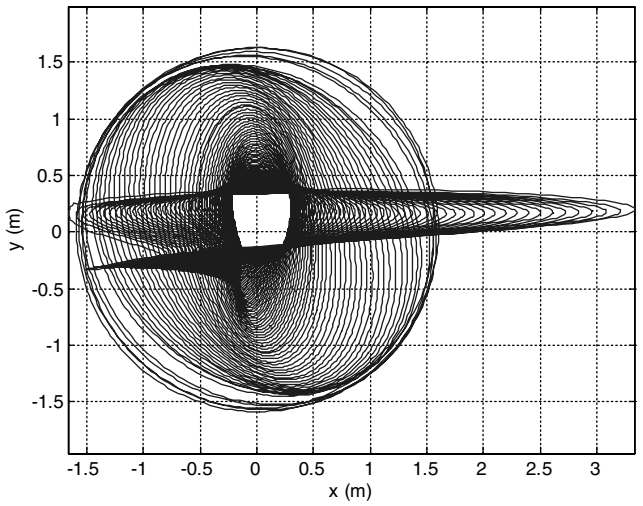

Fig. 20 Compensated projection of the orbit of cable tip in inertial frame with cable length fixed, shown in the horizontal plane (wind speed from 0 to 5 m/s).

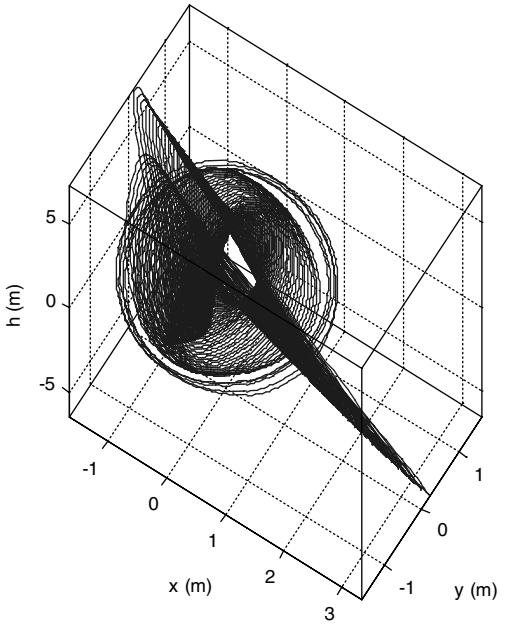

Fig. 21 Compensated orbit of cable tip in inertial frame with cable length fixed (wind speed from 0 to 5 m/s).

downwind direction. At 5 m/s, the maximum deviation is approximately 3.25 m. Hence, from the point of view of maintaining small motion of the cable tip, reeling the tether is preferable. Figure 21, which shows the three-dimensional trajectories of the cable tip, support this conclusion. Varying the altitude of the aircraft is unable to compensate for the vertical motion of the cable tip in the same fashion as cable reeling. This is because the cable tip motion tends to be damped with longer cables [16]. Peak-to-peak oscillations of approximately 10 m are present in the results for a wind speed of 5 m/s.

Figure 22 shows the shift in the aircraft orbit, Fig. 23 shows the eccentricity and ellipse orientation, and Fig. 24 shows the aircraft mean altitude and semimajor axis. In contrast to the results where reeling is used, the aircraft maintains a circular orbit for wind speeds above 1.5 m/s. The mean altitude of the aircraft decreases with wind speed. Figure 25 shows the variation in orbit altitude as a function of wind speed. This shows that the amplitude of oscillation for the aircraft altitude is substantially less than the required length of cable needed to stabilize the cable tip motion. This is consistent with the

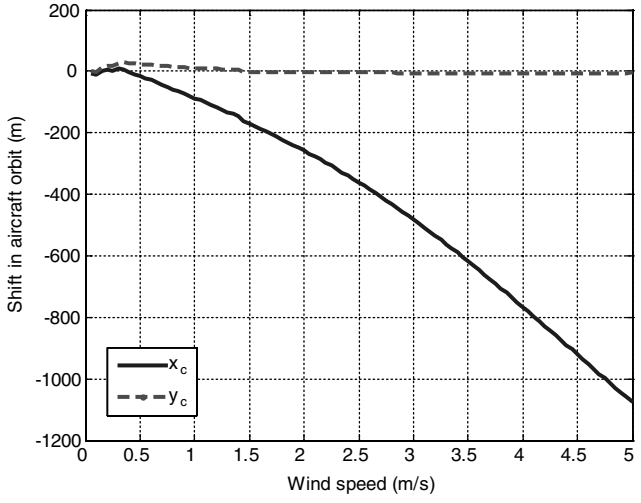

Fig. 22 Shift in aircraft orbit as a function of wind speed with cable length fixed.

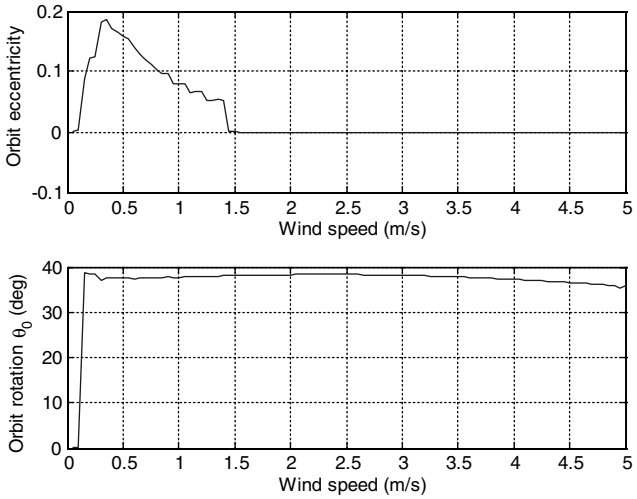

Fig. 23 Optimal orbit eccentricity and orientation of major axis of ellipse for compensating for effect of crosswind with length fixed.

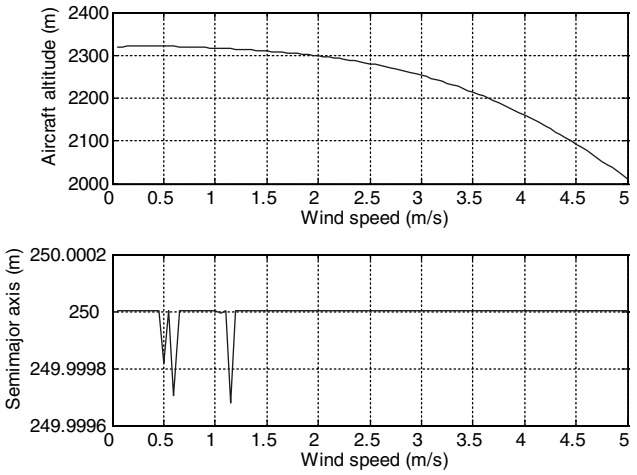

Fig. 24 Optimal aircraft altitude and semimajor axis for compensating for effect of crosswind with length fixed.

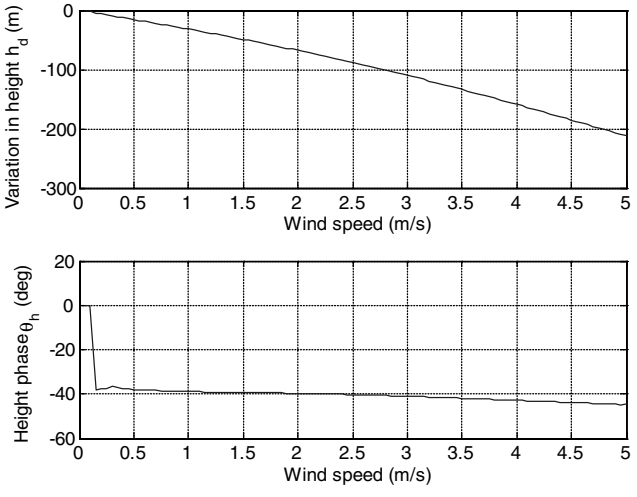

Fig. 25 Optimal variation and phasing of altitude to compensate for effects of cross wind.

periodic solutions generated earlier in this paper. The results show that although the variation in altitude is less effective in stabilizing the cable motion, it may be preferable since it would not require a complex interaction of autopilot with winch control. The price in accuracy would most likely be masked in practice due to the effects of turbulence and gusts.

The results presented above clearly illustrates that accurate control of the cable tip can indeed be maintained by flying the aircraft in an appropriate manner, combined with reeling of the cable. It is interesting to note that the change in wind speed actually enables a "closer" trajectory to the origin when viewed in the horizontal plane.

Thus, the form of the optimal trajectories appears to be consistent with findings of studies of periodic orbits in the presence of crosswinds as investigated earlier in this paper. Preliminary flight testing of such a system has also illustrated some of these effects, namely, that the tip of the cable oscillates in the vertical plane and drifts outside of the flight path of the aircraft [24]. However, it is clear that the required shifts in the aircraft orbit are very large, even for moderate crosswinds.

VII. Conclusions

The optimal dynamics of a three-dimensional towed-cable system has been studied using numerical optimal control. The system is highly complex and nonlinear, and a multibody dynamics model was used to develop the optimal trajectories. For the case of no wind, it is known that an aircraft flying a circular orbit produces an optimal steady-state solution—optimal in the sense that no active control over the cable length is required to keep the cable tip "close" to the center of the orbit. However, even a small crosswind creates a large disturbance to the position of the cable tip. Shifts in the aircraft orbit of over 1 km are needed for wind speeds of 5 m/s for a 2.5 km long, 2 mm diameter cable. Flying the aircraft in a slightly elliptical orbit and reeling the cable gives extremely good compensation of the cable tip motion. It is possible to achieve better stationary motion than can be achieved in the absence of a crosswind. From a practical point of view, it would be likely that a solution that uses only an autopilot without varying the cable length would be sought. Such stabilized solutions are possible by flying the aircraft on an inclined circular orbit. The performance in the horizontal plane is not as good as using reeling for high wind speeds, but has the advantage that all control can be realized through a single autopilot. The loss in performance would most likely be masked in practice due to the effects of unsteady winds.

Appendix A: Inertial Velocities and Accelerations

The inertial velocity of the lumped masses obtained by differentiating Eqs. (1) and (2) and are given by,

$$\begin{aligned}\boldsymbol{v}_1 &= (\dot{r} - \dot{l}_1 \sin\alpha_1 - l_1\dot{\alpha}_1 \cos\alpha_1 + l_1\dot{\theta}\cos\alpha_1 \sin\beta_1)\boldsymbol{i} \\ &+ (r\dot{\theta} - \dot{l}_1 \cos\alpha_1 \sin\beta_1 + l_1\dot{\alpha}_1 \sin\alpha_1 \sin\beta_1 \\ &- l_1\dot{\beta}_1 \cos\alpha_1 \cos\beta_1 - l_1\dot{\theta}\sin\alpha_1)\boldsymbol{j} \\ &+ (\dot{h} - \dot{l}_1 \cos\alpha_1 \cos\beta_1 + l_1\dot{\alpha}_1 \sin\alpha_1 \cos\beta_1 \\ &+ l_1\dot{\beta}_1 \cos\alpha_1 \sin\beta_1)\boldsymbol{k} \end{aligned} \tag{A1}$$

$$\begin{aligned}\boldsymbol{v}_j &= \boldsymbol{v}_{j-1} + (-\dot{l}_j \sin\alpha_j - l_j\dot{\alpha}_j \cos\alpha_j + l_j\dot{\theta}\cos\alpha_j \sin\beta_j)\boldsymbol{i} \\ &+ (-\dot{l}_j \cos\alpha_j \sin\beta_j + l_j\dot{\alpha}_j \sin\alpha_j \sin\beta_j - l_j\dot{\beta}_j \cos\alpha_j \cos\beta_j \\ &- l_j\dot{\theta}\sin\alpha_j)\boldsymbol{j} + (-\dot{l}_j \cos\alpha_j \cos\beta_j + l_j\dot{\alpha}_j \sin\alpha_j \cos\beta_j \\ &+ l_j\dot{\beta}_j \cos\alpha_j \sin\beta_j)\boldsymbol{k}, \qquad j = 2, \ldots n \end{aligned} \tag{A2}$$

The accelerations in the rotating frame are given by

$$
\begin{aligned}
\boldsymbol{a}_1 = {} & (\ddot{r} - r\dot{\theta}^2 - \ddot{l}_1 \sin\alpha_1 - 2\dot{l}_1\dot{\alpha}_1 \cos\alpha_1 - l_1\ddot{\alpha}_1 \cos\alpha_1 \\
& + l_1\dot{\alpha}_1^2 \sin\alpha_1 + 2\dot{l}_1\dot{\theta}\cos\alpha_1 \sin\beta_1 + l_1\ddot{\theta}\cos\alpha_1 \sin\beta_1 \\
& - 2l_1\dot{\theta}\dot{\alpha}_1 \sin\alpha_1 \sin\beta_1 + 2l_1\dot{\theta}\dot{\beta}_1 \cos\alpha_1 \cos\beta_1 + l_1\dot{\theta}^2 \sin\alpha_1)\boldsymbol{i} \\
& + (r\ddot{\theta} + 2\dot{r}\,\dot{\theta} - \ddot{l}_1 \cos\alpha_1 \sin\beta_1 + 2\dot{l}_1\dot{\alpha}_1 \sin\alpha_1 \sin\beta_1 \\
& - 2\dot{l}_1\dot{\beta}_1 \cos\alpha_1 \cos\beta_1 + l_1\ddot{\alpha}_1 \sin\alpha_1 \sin\beta_1 + l_1\dot{\alpha}_1^2 \cos\alpha_1 \sin\beta_1 \\
& + 2l_1\dot{\alpha}_1\dot{\beta}_1 \sin\alpha_1 \cos\beta_1 - l_1\ddot{\beta}_1 \cos\alpha_1 \cos\beta_1 \\
& + l_1\dot{\beta}_1^2 \cos\alpha_1 \sin\beta_1 - 2\dot{l}_1\dot{\theta}\sin\alpha_1 - l_1\ddot{\theta}\sin\alpha_1 \\
& - 2l_1\dot{\theta}\dot{\alpha}_1 \cos\alpha_1 + l_1\dot{\theta}^2 \cos\alpha_1 \sin\beta_1)\boldsymbol{j} \\
& + (\ddot{h} - \ddot{l}_1 \cos\alpha_1 \cos\beta_1 + 2\dot{l}_1\dot{\alpha}_1 \sin\alpha_1 \cos\beta_1 \\
& + 2\dot{l}_1\dot{\beta}_1 \cos\alpha_1 \sin\beta_1 + l_1\ddot{\alpha}_1 \sin\alpha_1 \cos\beta_1 \\
& + l_1\dot{\alpha}_1^2 \cos\alpha_1 \cos\beta_1 - 2l_1\dot{\alpha}_1\dot{\beta}_1 \sin\alpha_1 \sin\beta_1 \\
& + l_1\ddot{\beta}_1 \cos\alpha_1 \sin\beta_1 + l_1\dot{\beta}_1^2 \cos\alpha_1 \cos\beta_1)\boldsymbol{k}
\end{aligned} \tag{A3}
$$

$$
\begin{aligned}
\boldsymbol{a}_j = {} & \boldsymbol{a}_{j-1} + (-\ddot{l}_j \sin\alpha_j - 2\dot{l}_j\dot{\alpha}_j \cos\alpha_2 - l_j\ddot{\alpha}_j \cos\alpha_j + l_j\dot{\alpha}_j^2 \sin\alpha_j \\
& + 2\dot{l}_j\dot{\theta}\cos\alpha_j \sin\beta_j + l_j\ddot{\theta}\cos\alpha_j \sin\beta_j - 2l_j\dot{\theta}\dot{\alpha}_j \sin\alpha_j \sin\beta_j \\
& + 2l_j\dot{\theta}\dot{\beta}_j \cos\alpha_j \cos\beta_j + l_j\dot{\theta}^2 \sin\alpha_j)\boldsymbol{i} + (-\ddot{l}_j \cos\alpha_j \sin\beta_j \\
& + 2\dot{l}_j\dot{\alpha}_j \sin\alpha_j \sin\beta_j - 2\dot{l}_j\dot{\beta}_j \cos\alpha_j \cos\beta_j + l_j\ddot{\alpha}_j \sin\alpha_j \sin\beta_j \\
& + l_j\dot{\alpha}_j^2 \cos\alpha_j \sin\beta_j + 2l_j\dot{\alpha}_j\dot{\beta}_j \sin\alpha_j \cos\beta_j \\
& - l_j\ddot{\beta}_j \cos\alpha_j \cos\beta_j + l_j\dot{\beta}_j^2 \cos\alpha_j \sin\beta_j - 2\dot{l}_j\dot{\theta}\sin\alpha_j \\
& - l_j\ddot{\theta}\sin\alpha_j - 2l_j\dot{\theta}\dot{\alpha}_j \cos\alpha_j + l_j\dot{\theta}^2 \cos\alpha_j \sin\beta_j)\boldsymbol{j} \\
& + (-\ddot{l}_j \cos\alpha_j \cos\beta_j + 2\dot{l}_j\dot{\alpha}_j \sin\alpha_j \cos\beta_j \\
& + 2\dot{l}_j\dot{\beta}_j \cos\alpha_j \sin\beta_j + l_j\ddot{\alpha}_j \sin\alpha_j \cos\beta_j + l_j\dot{\alpha}_j^2 \cos\alpha_j \cos\beta_j \\
& - 2l_j\dot{\alpha}_j\dot{\beta}_j \sin\alpha_j \sin\beta_j + l_j\ddot{\beta}_j \cos\alpha_j \sin\beta_j \\
& + l_j\dot{\beta}_j^2 \cos\alpha_j \cos\beta_j)\boldsymbol{k}, \qquad j = 2, \ldots, n
\end{aligned} \tag{A4}
$$

Appendix B: Inelastic Constraints

The tension constraint equations are obtained by projecting the equations of motion into a tangent frame for each tether element. In the simplest form, they are given by

$$
b^T_{j,j-1}T_{j-1} + b^T_{j,j}T_j + b^T_{j,j+1}T_{j+1} = [C^t_r]_j\left(\boldsymbol{a}_{j|j-1} - \left[\frac{\boldsymbol{F}_j}{m_j} - \frac{\boldsymbol{F}_{j-1}}{m_{j-1}}\right]\right)\cdot\boldsymbol{i} \tag{B1}
$$

where the coefficients of the tensions in Eq. (B1) are given by

$$
\begin{aligned}
b^T_{j,j-1} = {} & \frac{\sin(\alpha_j)\sin(\alpha_{j-1})}{m_{j-1}} + \frac{\cos(\alpha_j)\sin(\beta_j)\cos(\alpha_{j-1})\sin(\beta_{j-1})}{m_{j-1}} \\
& + \frac{\cos(\alpha_j)\cos(\beta_j)\cos(\alpha_{j-1})\cos(\beta_{j-1})}{m_{j-1}}
\end{aligned} \tag{B2}
$$

$$
\begin{aligned}
b^T_{j,j} = {} & -\sin(\alpha_j)\left(\frac{\sin(\alpha_j)}{m_j} + \frac{\sin(\alpha_j)}{m_{j-1}}\right) \\
& - \cos(\alpha_j)\sin(\beta_j)\left(\frac{\cos(\alpha_j)\sin(\beta_j)}{m_j} + \frac{\cos(\alpha_j)\sin(\beta_j)}{m_{j-1}}\right) \\
& - \cos(\alpha_j)\cos(\beta_j)\left(\frac{\cos(\alpha_j)\cos(\beta_j)}{m_j} + \frac{\cos(\alpha_j)\cos(\beta_j)}{m_{j-1}}\right)
\end{aligned} \tag{B3}
$$

$$
\begin{aligned}
b^T_{j,j+1} = {} & \frac{\sin(\alpha_j)\sin(\alpha_{j+1})}{m_j} + \frac{\cos(\alpha_j)\sin(\beta_j)\cos(\alpha_{j+1})\sin(\beta_{j+1})}{m_j} \\
& + \frac{\cos(\alpha_j)\cos(\beta_j)\cos(\alpha_{j+1})\cos(\beta_{j+1})}{m_j}
\end{aligned} \tag{B4}
$$

Applying Eq. (B1) for each tether element results in a set of linear algebraic equations for the n unknown tensions. Boundary conditions are applied by setting $T_0 = 0$, $T_{n+1} = 0$, and $m_0 = \infty$.

References

[1] Kolodner, I., "Heavy Rotating String: A Nonlinear Eigenvalue Problem," *Communications on Pure and Applied Mathematics*, Vol. 9, 1955, pp. 334–338.

[2] Caughey, T. K., "Whirling of a Heavy Chain," *Proceedings of the Third U. S. National Congress of Applied Mechanics*, American Society of Mechanical Engineers, Fairfield, NJ, 1955, pp. 61–108.

[3] Skop, R. A., and Choo, Y.-I., "The Configuration of a Cable Towed in a Circular Path," *Journal of Aircraft*, Vol. 8, No. 11, 1971, pp. 856–862.

[4] Wu, C. H., "Whirling of a String at Large Angular Speeds—A Nonlinear Eigenvalue Problem with Moving Boundary Layers," *Journal of Applied Mathematics*, Vol. 22, No. 1, 1972, pp. 1–13.

[5] Russell, J. J., and Anderson, W. J., "Equilibrium and Stability of a Whirling Rod-Mass System," *International Journal of Non-Linear Mechanics*, Vol. 12, 1977, pp. 91–101.

[6] Russell, J. J., and Anderson, W. J., "Equilibrium and Stability of a Circularly Towed Cable Subject to Aerodynamic Drag," *Journal of Aircraft*, Vol. 14, No. 7, 1977, pp. 680–686.

[7] Zhu, F., and Rahn, C. D., "Stability Analysis of a Circularly Towed Cable-Body System," *Journal of Sound and Vibration*, Vol. 217, No. 3, 1998, pp. 435–452.

[8] Coomer, J., Lazarus, M., Tucker, R. W., Kershaw, D., and Tegman, A., "A Non-Linear Eigenvalue Problem Associated with Inextensible Whirling Strings," *Journal of Sound and Vibration*, Vol. 239, No. 5, 2001, pp. 969–982.

[9] Lemon, G., and Fraser, W. B., "Steady-State Bifurcations and Dynamical Stability of a Heavy Whirling Cable Acted on by Aerodynamic Drag," *Proceedings of the Royal Society of London, Series A: Mathematical and Physical Sciences*, Vol. 457, 2001, pp. 1021–1041.

[10] Williams, P., and Trivailo, P., "Cable Deployment Control for Towed Aerial-Cable Payload Pick-Up and Delivery System," *Proceedings of the Land Warfare Conference*, edited by Puri, V., Filippidis, D., Retter, P., and Kelly, J., Land Warfare Conference, Melbourne, Australia, Sept. 2004, pp. 313–329.

[11] Cochran, J. E., Innocenti, M., No., T. S., and Thukral, A., "Dynamics and Control of Maneuverable Towed Flight Vehicles," *Journal of Guidance, Control, and Dynamics*, Vol. 15, No. 5, 1992, pp. 1245–1252.

[12] Henderson, J. F., Potjewyd, J., and Ireland, B., "The Dynamics of an Airborne Towed Target System with Active Control," *Proceedings of the Institution of Mechanical Engineers*, Vol. 213, No. 5, 1999, pp. 305–319.

[13] Bourmistrov, A. S., Hill, R. D., and Riseborough, P., "Nonlinear Control Law for Aerial Towed Target," *Journal of Guidance, Control, and Dynamics*, Vol. 18, No. 6, 1995, pp. 1232–1238.

[14] Quisenberry, J. E., and Arena, A. S., "Dynamic Simulation of Low Altitude Aerial Tow Systems," *AIAA Atmospheric Flight Mechanics Conference and Exhibit*, AIAA Paper 2004-4813, Aug. 2004.

[15] Williams, P., and Trivailo, P., "Cable-Supported Sliding Payload Deployment from a Circling Fixed-Wing Aircraft," *Journal of Aircraft*, Vol. 43, No. 5, 2006, pp. 1567–1570.

[16] Williams, P., and Trivailo, P., "Dynamics of Circularly-Towed Aerial Cable Systems, Part I: Optimal Equilibrium Configurations and Their Stability," *Journal of Guidance, Control, and Dynamics*, Vol. 29, No. 6, Nov.–Dec. 2006.

[17] Williams, P., and Trivailo, P., "Dynamics of Circularly-Towed Aerial Cable Systems, Part II: Transitional Flight and Deployment Control," *Journal of Guidance, Control, and Dynamics*, Vol. 30, No. 3, May–June 2007.

[18] Murray, R. M., "Trajectory Generation for a Towed Cable System using Differential Flatness," *IFAC World Congress*, International Federation of Automatic Control, San Francisco, July 1996, pp. 395–400.

[19] Williams, P., and Trivailo, P., "Periodic Solutions for Flexible Cable-Body Systems Towed in Circular and Elliptical Paths," *AIAA Atmospheric Flight Mechanics Conference*, AIAA Paper 2006-6374, Aug. 2006.

[20] Borst, R. G., Greisz, G. F., and Quynn, A. G., "Fuzzy Logic Control Algorithm for Suppressing E-6A Long Trailing Wire Antenna Wind Shear Induced Oscillations," AIAA Paper 93-3868, Aug. 1993.

[21] Brushwood, D. L. J., Olson, A. P., and Smyth, J. M., "The E-6A Orbit Improvement System and its Effect Upon LTWA Verticality," AIAA Paper 98-4426, Aug. 1998.

[22] Williams, P., "Periodic Optimal Control of a Circularly-Towed Aerial-Cable System in Presence of Cross-Wind," *AIAA Guidance, Navigation, and Control Conference*, AIAA Paper 2006-6192, 21–24 August 2006.

[23] Hoerner, S. F., *Fluid-Dynamic Drag*, published by the author, 1965.

[24] Williams, P., Lapthorne, P., and Trivailo, P., "Circularly-Towed Lumped Mass Cable Model Validation from Experimental Data," *AIAA Modeling and Simulation Conference*, AIAA Paper 2006-6817, Aug. 2006.

[25] Gill, P. E., Murray, W., and Saunders, M. A., "SNOPT: An SQP Algorithm for Large-Scale Constrained Optimization," *SIAM Journal on Optimization*, Vol. 12, No. 4, 2002, pp. 979–1006.